Journal of Physical Science
Vol. 37(2), 1–16, 2026

Impacts of Radiation and Chemical Reactions on Magnetohydrodynamics Thermosolutal Convection in a Porous Cylindrical Cavity Incorporating the Soret and Dufour Effects

Mustapha El Hamma,[1*] Mohammed Taibi,[1,2] Ahmed Rtibi[1] and Kamal Gueraoui[1]

[1]Physics Department, Team of Modelling and Simulation in Mechanics and Energetics (MSME), Faculty of Sciences, Mohammed V University in Rabat, 4 Avenue Ibn Batouta, BP 1014, Rabat 10000, Morocco
[2]Labo of Mechanics, Faculty of Sciences Aïn Chock, University of Hassan II of Casablanca, Km 8 Route d'El Jadida, B.P. 5366 Maârif, Casablanca 20100, Morocco

*Corresponding author: mustapha_elhamma@um5.ac.ma

Published online: 28 August 2026

To cite this article: El Hamma, M. et al. (2026). Impacts of radiation and chemical reactions on magnetohydrodynamics thermosolutal convection in a porous cylindrical cavity incorporating the Soret and Dufour effects. *J. Phys. Sci.*, 37(2), 1–16. https://doi.org/10.21315/jps2026.37.2.1

To link to this article: https://doi.org/10.21315/jps2026.37.2.1

ABSTRACT: The objective of this study is to numerically and theoretically model the coupled heat and mass transfer in a porous, isotropic and saturated medium filled with a Casson nanofluid containing aluminium nanoparticles, taking into account the effects of radiation, chemical reactions, a magnetic field and the Soret and Dufour effects. The analysis is conducted for various parameters relevant to the model, including the chemical reaction parameter (ranging from 0–20), the radiation parameter (0–2), the Casson fluid parameter (0.1–1), the Soret and Dufour numbers (0–1), the conductivity ratio (1–3), the Hartmann number (0–100) and the thrust ratio (1–2). The horizontal boundaries of the cavity are maintained at constant temperature and concentration, while the vertical walls are assumed to be rigid, impermeable and adiabatic. The flow of the Casson nanofluid in the porous medium is governed by the extended Brinkman–Forchheimer–Darcy law. The system of equations is solved using the finite volume method. The findings reveal that the heat transfer rate increases with the chemical reaction parameter, geometric aspect ratio, Casson fluid parameter, thermal conductivity and thrust ratio. Conversely, the heat transfer rate decreases with higher Hartmann and Dufour numbers. Regarding mass transfer, it increases with higher thermal conductivity, thrust ratio and geometric aspect ratio, but decreases with higher Hartmann number, Soret effect and chemical reaction parameter.

Keywords: Casson nanofluid, chemical reaction, radiation, Soret and Dufour effect, MHD

© Penerbit Universiti Sains Malaysia, 2026. This work is licensed under the terms of the Creative Commons Attribution (CC BY) (http://creativecommons.org/licenses/by/4.0/).

1. INTRODUCTION

The influence of chemical reactions on heat and mass transfer processes plays a crucial role in a variety of applications, including drying, evaporation from water bodies and flow in desert coolers. Such flows are also significant in numerous industrial, geophysical and engineering contexts, which has stimulated increased research interest in recent years. Chemical reactions can be categorised as either heterogeneous or homogeneous processes. Consequently, there has been growing attention on modelling double-diffusive convection in porous media.[1]

Numerous studies have aimed to elucidate the fundamental mechanisms of heat and mass transfer in double-diffusive convection within porous media. For example, Zhang et al. examined Marangoni thermosolutal convection with heat generation and first-order chemical reactions.[2] Al-Mudhaf et al. explored similarity solutions for Marangoni thermosolutal convection over flat surfaces under the effects of heat generation or absorption.[3] El Hamma et al. conducted theoretical and numerical investigations of thermosolutal convection in cylindrical porous cavities filled with nanofluids, accounting for the Soret and Dufour effects.[4,5] Other notable contributions include Al-Sulaimi et al., who investigated nonlinear energy stability in Brinkman thermosolutal convection with chemical reactions.[6] Mohamed et al. analysed the impact of thermal radiation and chemical reactions on free convective flow of polar fluids through porous media with internal heat generation.[7] El Hamma et al. also examined the influence of radiation absorption and the Soret and Dufour effects on magnetohydrodynamics (MHD) thermosolutal convection in a porous cylindrical cavity filled with Casson nanofluid.[8] Qadan et al. studied MHD mixed convection heat transfer for a horizontal circular cylinder embedded in a micropolar Casson fluid with thermal radiation.[9] Sharma et al. investigated the effects of homogeneous and heterogeneous chemical reactions on non-Newtonian fluids around a permeable, inclined, stretching cylinder.[10] Similarly, Patil et al. and Elattari et al. analysed the influence of chemical reactions on free convective flows through porous media and cylindrical cavities filled with Casson fluid, incorporating the Soret and Dufour effects.[11,12] Laxmaiah et al. investigated the influence of thermal radiation and chemical reactions on the MHD flow of a Williamson nanofluid over an exponentially porous stretching sheet in the presence of a non-uniform heat source and sink.[13] Ahad et al. investigated MHD thermosolutal convection of hybrid nanofluids along a vertical corrugated surface with wall heat and mass flux.[14] El Haroui et al. predicted thermosolutal convection in porous media, incorporating Soret–Dufour and chemical reaction effects.[15] The work of El Hamma et al. and Choukairy et al. focused on similar modelling of convection in porous cavities with Casson nanofluids, alongside numerical and analytical analysis of heterogeneous porous media convection.[16,17] other significant contributions include studies by Venkatadri et al., Swapna et al. and Hussein et al., who explored various aspects of MHD convection and nanofluid behaviour in different porous media and geometries.[18–20] Essalhi et al. compared the thermal performance of two solar air collectors for an indirect solar dryer.[21] Zhu et al. investigated numerical methods for unsteady convection–diffusion problems, combining compact difference schemes with Runge–Kutta methods.[22] Bin Turabi et al. studied natural convective flow of hybrid nanofluid in a triangular enclosure with a heated wavy wall and a cold obstacle.[23] Ahmad et al. conducted numerical simulations of MHD double-diffusive natural convection in a cavity with non-uniformly heated walls.[24] Munir et al. performed computational analyses of thermal enhancement and flow dynamics in lid-driven staggered cavities with uniform and non-uniform temperature walls.[25]

The present study distinguishes itself by modelling coupled heat and mass transfer within a porous cylindrical cavity saturated with a Casson nanofluid composed of a binary base fluid. This work incorporates the effects of radiation absorption, chemical reactions, thermodiffusion (Soret and Dufour effects) and the influence of a vertically aligned magnetic field.

2. FORMULATION OF THE PROBLEM

2.1 Geometry of the Flow

A cylindrical enclosure filled with an isotropic porous medium and saturated with a Casson nanofluid is employed to investigate the phenomenon of thermosolutal convection. Both the lower and upper bases of the enclosure (see Figure 1) are maintained at uniform temperatures and concentrations, while the side walls are assumed to be adiabatic and impermeable. The results are obtained under the following assumptions: steady-state flow, the use of a non-Newtonian fluid, symmetry and two-dimensional flow, and a laminar and stable flow field. The Boussinesq approximation is applied to model density variations, and the thermophysical properties of the base fluid and nanoparticles (aluminium nanoparticles) are considered constant. Furthermore, the nanoparticles are assumed to be uniformly distributed within the base fluid, with consistent size and shape. Thermal equilibrium is assumed between the base fluid and nanoparticles, with no slip between the two phases and viscous dissipation is neglected.

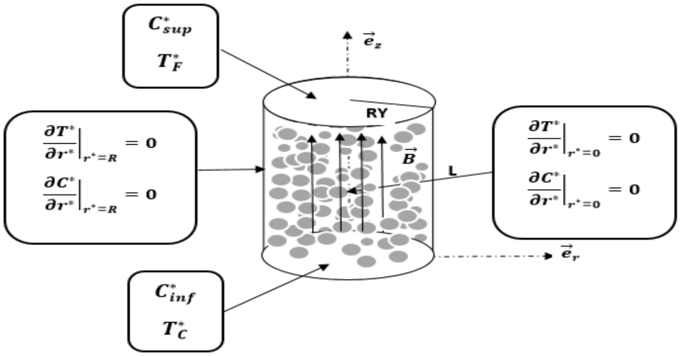

Figure 1: Geometrical configuration of the problem under study.

2.2 Dimensional Governing Equations

The mathematical description of the studied phenomenon is provided by the conservation equations of continuum mechanics. The flow of the nanofluid within the porous medium is governed by the Darcy–Brinkman–Forchheimer equations.

2.2.1 Continuity equation

The continuity equation in dimensional form is expressed as:

$$\frac{1}{r^*}\frac{\partial\left(r^* u^*\right)}{\partial r^*}+\frac{\partial w^*}{\partial z^*}=0 \tag{1}$$

2.2.2 Momentum conservation equation

The momentum conservation equation in dimensional form is expressed as:

$$\begin{aligned}
&\frac{1}{\varepsilon^2}\left(\frac{1}{r^*}\frac{\partial(r^* u^* \Omega^*)}{\partial r^*}+\frac{\partial(w^*\Omega^*)}{\partial z^*}-\frac{u^*\Omega^*}{r^*}\right)\\
&\qquad=-\frac{\mu_{nf}}{\mathrm{K}\rho_{0nf}}\Omega^*-\frac{\rho_0(1-\varphi)}{\rho_{0nf}}\beta_{\mathrm{T}}g\frac{\partial \mathrm{T}^*}{\partial r^*}\\
&\qquad-\frac{\rho_0(1-\varphi)}{\rho_{0nf}}\beta_{\mathrm{S}}g\frac{\partial C^*}{\partial r^*}+\frac{\mu_{nf}}{\varepsilon\rho_{0nf}}\left(1+\frac{1}{\beta}\right)\\
&\qquad\left(\frac{\partial^2\Omega^*}{\partial r^{*2}}+\frac{1}{r^*}\frac{\partial\Omega^*}{\partial r^*}+\frac{\partial^2\Omega^*}{\partial z*^2}-\frac{\Omega^*}{r*^2}\right)-\frac{C_F}{K^{\frac{1}{2}}}\\
&\qquad|\vec{\mathrm{V}}^*|\Omega^*+\frac{C_F}{K^{\frac{1}{2}}}\left(w^*\frac{\partial|\vec{\mathrm{V}}^*|}{\partial z^*}-u^*\frac{\partial|\vec{\mathrm{V}}^*|}{\partial z^*}\right)-\frac{1}{\rho_{0nf}}\sigma_{nf}B^2\frac{\partial u^*}{\partial z^*}
\end{aligned} \tag{2}$$

2.2.3 Conservation of energy equation

The energy conservation equation in dimensional form is expressed as:

$$\left(\frac{\partial(u^{*}T^{*})}{\partial r^{*}}+\frac{\partial(w^{*}T^{*})}{\partial z^{*}}+\frac{u^{*}T^{*}}{r^{*}}\right)$$
$$=\alpha\left(\frac{\partial^{2}T^{*}}{\partial r^{*2}}+\frac{\partial^{2}T^{*}}{\partial z^{*2}}+\frac{1}{r^{*}}\frac{\partial T^{*}}{\partial r^{*}}\right)+\varepsilon\, k_{TC} \tag{3}$$
$$\left(\frac{\partial^{2}C^{*}}{\partial r*^{2}}+\frac{\partial^{2}C^{*}}{\partial z*^{2}}+\frac{1}{r^{*}}\frac{\partial C^{*}}{\partial r^{*}}\right)-\frac{\alpha}{X_{e}}\nabla q$$

For optically thick nanofluids exhibiting self-absorption, the radiative heat flux in the energy equation is modelled using the Rosseland approximation, as follows:

$$q=-\frac{4\bar{\sigma}\nabla T^{4}}{3\delta} \tag{4}$$

We assume that the temperature variations within both the fluid and the porous medium are small enough for T^4 to be approximated as a linear function of temperature around a reference temperature T_0 using a Taylor expansion. Higher-order terms are neglected, yielding the following expression:

$$T^{4}\approx 4T_{0}^{3}T-3T_{0}^{3} \tag{5}$$

So

$$q=-\frac{16\bar{\sigma}}{3\delta}T_{0}^{3}\nabla\mathrm{T} \tag{6}$$

$$\left(\frac{\partial(u^{*}T^{*})}{\partial r^{*}}+\frac{\partial(w^{*}T^{*})}{\partial z^{*}}+\frac{u^{*}T^{*}}{r^{*}}\right)$$
$$=\alpha\left(\frac{\partial^{2}T^{*}}{\partial r*^{2}}+\frac{\partial^{2}T^{*}}{\partial z*^{2}}+\frac{1}{r^{*}}\frac{\partial T^{*}}{r^{*}\partial r^{*}}\right)+\varepsilon\, k_{TC}$$
$$\left(\frac{\partial^{2}C^{*}}{\partial r*^{2}}+\frac{\partial^{2}C^{*}}{\partial z*^{2}}+\frac{1}{r^{*}}\frac{\partial C^{*}}{\partial r^{*}}\right)+\frac{\alpha}{X_{e}}\frac{16\bar{\sigma}}{3\delta}T_{0}^{3} \tag{7}$$
$$\left(\frac{\partial^{2}T^{*}}{\partial r*^{2}}+\frac{\partial^{2}T^{*}}{\partial z*^{2}}+\frac{1}{r^{*}}\frac{\partial T^{*}}{r^{*}\partial r^{*}}\right)$$

2.2.4 Conservation of concentration equation

The concentration conservation equation in dimensional form is expressed as:

$$\left(\frac{\partial(u^*C^*)}{\partial r^*}+\frac{\partial(w^*C^*)}{\partial z^*}+\frac{u^*C^*}{r^*}\right) \\ = \mathrm{D}\,\varepsilon\left(\frac{\partial^2 C^*}{\partial r*^2}+\frac{\partial^2 C^*}{\partial z*^2}+\frac{1}{r^*}\frac{\partial C^*}{\partial r^*}\right)+\varepsilon\, k_{CT} \\ \left(\frac{\partial^2 T^*}{\partial r*^2}+\frac{\partial^2 T^*}{\partial z*^2}+\frac{1}{r^*}\frac{\partial T^*}{\partial r^*}\right)-\Lambda(C^*-C^*{}_F) \tag{8}$$

2.2.5 The current function equation

The current function equation in dimensional form is expressed as:

$$u^*=\frac{1}{r^*}\frac{\partial\psi^*}{\partial z^*} \tag{9}$$

$$w^*=-\frac{1}{r^*}\frac{\partial\psi^*}{\partial r^*} \tag{10}$$

$$\Omega^*=\frac{1}{r^*}\left(\Delta\psi^*-\frac{2}{r^*}\frac{\partial\psi^*}{\partial z^*}\right) \tag{11}$$

2.3 Dimensionless Equations

The previously derived equations are expressed in dimensionless form as:

$$\frac{1}{r}\frac{\partial(ru)}{\partial r}+\frac{\partial w}{\partial z}=0 \tag{12}$$

$$\frac{1}{\varepsilon^2}\left(\frac{1}{r}\frac{\partial(rU\Omega)}{\partial r}+\frac{\partial(W\Omega)}{\partial z}-\frac{U\Omega}{r}\right) \\ =-X\frac{Pr_{nf}}{Da}\Omega-X^2R_{T,nf}Pr_{nf}\left(\frac{\partial T}{\partial r}+N\frac{\partial C}{\partial r}\right) \\ +\frac{XPr_{nf}}{\varepsilon}\left(1+\frac{1}{\beta}\right)\left(\frac{\partial^2\Omega}{\partial r^2}+\frac{1}{r}\frac{\partial\Omega}{\partial r}+\frac{\partial^2\Omega}{\partial z^2}-\frac{\Omega}{r^2}\right) \\ -\frac{C_F}{\sqrt{Da}}|\vec{V}|\Omega+\frac{C_F}{\sqrt{Da}}\left(W\frac{\partial|\vec{V}|}{\partial\bar{r}}-U\frac{\partial|\vec{V}|}{\partial\bar{z}}\right) \\ -XPr_{nf}Ha^2\frac{\partial U}{\partial Z} \tag{13}$$

$$\left(\frac{\partial(UT)}{\partial r}+\frac{\partial(WT)}{\partial z}+\frac{UT}{r}\right)$$
$$=(1+R^{2})\left(\frac{\partial^{2}T}{\partial r^{2}}+\frac{\partial^{2}T}{\partial z^{2}}+\frac{1}{r}\frac{\partial T}{\partial r}\right)$$
$$+\varepsilon Du\left(\frac{\partial^{2}C}{\partial r^{2}}+\frac{\partial^{2}C}{\partial z^{2}}+\frac{1}{r}\frac{\partial C}{\partial r}\right) \tag{14}$$

$$\left(\frac{\partial(UC)}{\partial r}+\frac{\partial(WC)}{\partial z}+\frac{UC}{r}\right)$$
$$=\frac{\varepsilon}{Le}\left[\left(\frac{\partial^{2}C}{\partial r^{2}}+\frac{\partial^{2}C}{\partial z^{2}}+\frac{1}{r}\frac{\partial C}{\partial r}\right)+Sr\left(\frac{\partial^{2}T}{\partial r^{2}}+\frac{\partial^{2}T}{\partial z^{2}}+\frac{1}{r}\frac{\partial T}{\partial r}\right)\right]-\zeta C \tag{15}$$

$$\mathrm{U}=\frac{1}{r}\frac{\partial\psi}{\partial z} \tag{16}$$

$$W=-\frac{1}{r}\frac{\partial\psi}{\partial r} \tag{17}$$

$$\Omega=\frac{1}{r}\frac{\partial^{2}\psi}{\partial r^{2}}-\frac{1}{r^{2}}\frac{\partial\psi}{\partial r}+\frac{1}{r}\frac{\partial^{2}\psi}{\partial z^{2}} \tag{18}$$

By defining the following dimensionless variables :

$$U=\frac{u^{*}RY}{\alpha},W=\frac{w^{*}RY}{\alpha},\Omega=\frac{\Omega^{*}RY^{2}}{\alpha},\psi=\frac{\psi^{*}}{\mathrm{RY}\alpha},T=\frac{T^{*}-T^{*}{}_{F}}{T^{*}{}_{C}-T^{*}{}_{F}},C=\frac{C^{*}-C^{*}{}_{sup}}{C^{*}{}_{inf}-C^{*}{}_{sup}}$$

The following dimensionless parameters are defined:

$$R_{T,nf}=\frac{\rho_{0}\left(1-\varphi\right)g\ \beta_{\mathrm{T}}\Delta TRY^{3}}{\mu_{nf}\alpha_{nf}},Pr_{nf}=\frac{\upsilon_{nf}}{\alpha_{nf}},Da=\frac{K}{RY^{2}},\mathrm{N}=\frac{\beta_{C}\Delta C}{\beta_{T}\Delta T},Le=\frac{\alpha}{D},$$
$$Du=\frac{K_{TC}\Delta C}{\alpha\Delta T},Sr=\frac{K_{CT}\Delta T}{D\Delta C},X=\frac{Xnf}{Xe},\xi=\frac{RY\Lambda}{\alpha},R=\left(\frac{16\bar{\sigma}T_{0}^{3}}{3\delta Xe}\right)^{1/2}$$

2.4 Dimensionless Boundary Conditions

$$r=0,\psi=0,\frac{\partial T}{\partial r}|_{r=0}=0,\frac{\partial C}{\partial r}|_{r=0}=0,\Omega|_{r=0}=0 \tag{19}$$

$$r=1,\psi=\frac{\partial\psi}{\partial r}=0,\frac{\partial T}{\partial r}|_{r=1}=0,\frac{\partial C}{\partial r}|_{r=1}=0,\Omega|_{r=1}\frac{2}{dr^{2}}\psi|_{r=1-\Delta r} \tag{20}$$

$$z=0,\psi=\frac{\partial\psi}{\partial r}=\frac{\partial\psi}{\partial z}=0,T=1,C=1,\Omega|_{z=0}\frac{1}{r}\frac{2}{dr^{2}}\psi|_{z=dz} \tag{21}$$

$$z=\mathrm{A},\psi=\frac{\partial\psi}{\partial r}=\frac{\partial\psi}{\partial z}=0,T=0,C=0,\Omega|_{z=\mathrm{A}}\frac{1}{r}\frac{2}{dz^{2}}\psi|_{z=A-dz} \tag{22}$$

2.5 Heat and Mass Transfer

The following relations describe the average heat and mass transfer at the horizontal active wall: the Nusselt number (Nu) and the Sherwood number (Sh).

$$Nu = -2A\int_0^1 \left.\frac{\partial T}{\partial z}\right|_{z=0} dr \tag{23}$$

$$Sh = -2A\int_0^1 \left.\frac{\partial C}{\partial z}\right|_{z=0} dr \tag{24}$$

3. RESOLUTION PROCESS

3.1 Resolution Method

Thermosolutal convection is a phenomenon governed by a system of strongly coupled, nonlinear partial differential equations, which precludes an analytical solution. This necessitates the use of numerical methods. In the present study, the finite volume method is employed.[26,27] The resulting algebraic equations are solved using the double sweep technique, with the boundary conditions fully incorporated. To solve the current function equation, the Simultaneous Over-Relaxation method is applied.[28,29] The convergence coefficient is expressed as follows:

$$\frac{\sum_i\sum_j\left|F_{i,j}^{n+1} - F_{i,j}^{n}\right|}{\sum_i\sum_j\left|F_{i,j}^{n+1}\right|} \leq 10^{-5} \tag{25}$$

3.2 Validation of Results

A grid convergence test in a Fortran code is conducted across multiple grid levels, with the following parameters held constant: Hartmann number (Ha) = 0, buoyancy ratio (N) = 1, geometric aspect ratio (A) = 3, Prandtl number (Pr) = 6.8, Lewis number (Le) = 2.5, volume fraction of nanoparticles (φ) = 0.05, Darcy number radiation parameter (Da) = 0.001, R = 0.5, Casson fluid parameter (β) = 0.1, conductivity ratio (χ) = 1, chemical reaction parameter (ξ) = 5, Soret number (Sr) = 1 and Dufour number (Du) = 1. The results are presented in Table 1. For this analysis, the average heat and mass fluxes are calculated. The results show that at a grid size 161 × 161, the solution converges.

Table 1: Grid independency study

Size of the grid	Nu	Error %
131 × 131	2.75010084081	0.33
141 × 141	2.74099083980	0.1
151 × 151	2.73810083970	$4.3 \times 10_{-3}$
161 × 161	2.73798084076	$4.3 \times 10_{-3}$
171 × 171	2.73786310759	–

The results obtained are in excellent agreement with those of authors who have addressed the same problem.[16] This comparison is based on the average Nusselt number as a function of the Casson fluid parameter, under the following conditions: A = 3, Thermal Rayleigh number of the nanofluid ($R_{T,nf}$) = 10^4, N = 1, Pr_{nf} = 6.8, Le = 2.5, φ = 0.05, Da = 0.001, χ = 1, ξ = 0, R = 0, Sr = 1 *et*, Du = 1, as shown in Table 2.

Table 2: Comparison of the numerical procedure with reference[16]

β	Nu [16]	Sh [16]	Nu (This study)	Sh (This study)
0.1	2.71589	2.67435	2.71357	2.67419
0.2	2.72472	2.68326	2.72357	2.68322
0.4	2.72808	2.68668	2.72516	2.68352
0.6	2.72913	2.68774	2.72813	2.68480
0.8	2.72964	2.68826	2.72851	2.68720
1.0	2.72995	2.68857	2.72663	2.68850

4. RESULTS AND DISCUSSION

4.1 Impact of the Chemical Reaction Parameter, Soret and Dufour Effect

The influence of the chemical reaction parameter and the Soret effect on heat and mass transfer is illustrated in Figure 2. The parameters are set as follows: A = 3, $R_{T,nf}$ = 10^4, N = 1, Prandtl number of the nanofluid (Pr_{nf}) = 6.8, Le = 2.5, φ = 0.05, Da = 0.001, β = 0.5, χ = 1, R = 1, Ha = 50, Du = 1.

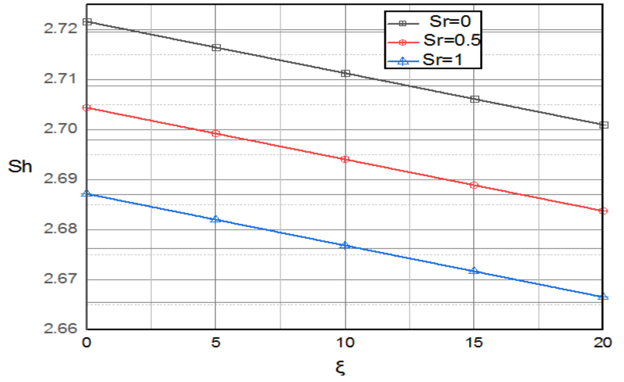

Figure 2: The effect ξ and Sr on the Sherwood Number (Sh).

With the chemical reaction parameter varying from 0–20 and the Soret effect ranging from 0–1, it can be observed from this figure that mass transfer decreases as the chemical reaction parameter increases. This reduction in mass transfer is attributed to the decline in species concentration caused by the chemical reaction, which weakens the concentration-driven buoyancy effects. Consequently, the flow rate within the cavity is reduced, leading to a further decrease in mass transfer. Conversely, an increase in the Soret coefficient, which governs the thermodiffusion phenomenon, also results in a reduction in mass transfer.

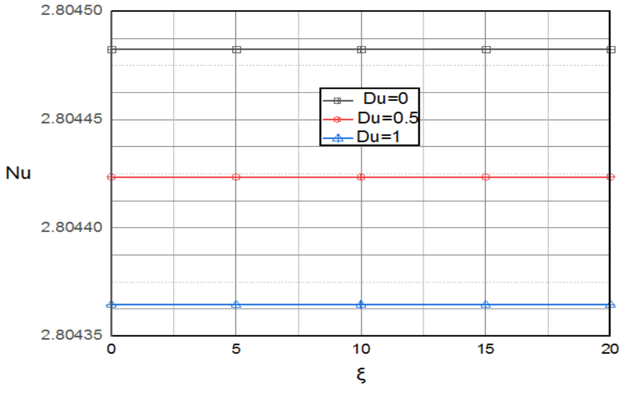

Figure 3: The effect of ξ and Du on the Nusselt Number (Nu).

Figure 3 illustrates the effect of the chemical reaction parameter and the Soret effect on heat transfer, with the parameters set as follows: A = 3 , $R_{T,nf} = 10^4$, $N = 1$, $Pr_{nf} = 6.8$, Le = 2.5, $\varphi = 0.05$, $Da = 0.001$, $\beta = 0.5$, $\chi = 1$, $R = 1$, $Ha = 50$, $Sr = 1$. The results indicate that heat transfer is largely unaffected by the chemical reaction parameter.

However, it is observed that heat transfer decreases with an increase in the Soret number, which characterises the thermodiffusion phenomenon. This reduction is attributed to the influence of thermodiffusion as the Soret number increases.

4.2 Influence of Radiation Parameter, Casson Fluid Parameter and Hartmann Number

Figures 4 and 5 illustrate the effect of the radiation parameter, Casson fluid parameter and Hartmann number on heat and mass transfer, with the parameters set as follows: A = 3, RT_{nf}=10^4, N = 1, Pr_{nf} = 6.8, Le = 2.5, φ = 0.05, Da = 0.001, χ = 1, ξ = 5, R = 1, Sr = 1, Du =1.

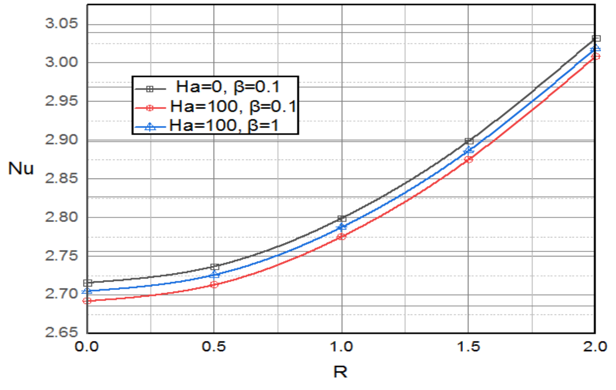

Figure 4: The effect of R, Ha and β on the Nusselt Number (Nu).

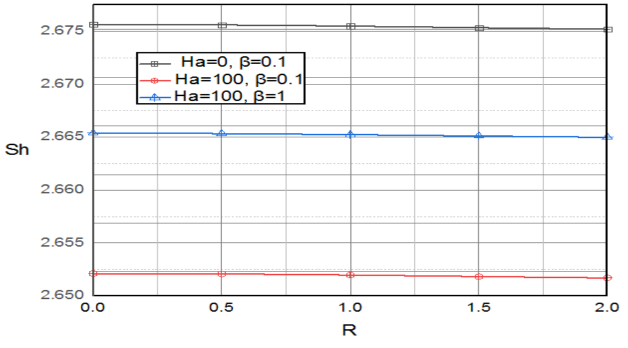

Figure 5: The effect of R, Ha and β on the Sherwood Number (Sh).

It is observed that heat transfer increases with the radiation parameter (R), which can be attributed to the enhanced intensity of the radiative flux as R increases. In contrast, mass transfer decreases slightly with increasing R, due to the intensified thermodiffusion phenomenon. Both heat and mass transfer are also found to increase with the Casson fluid parameter (β), as this enhancement in thermosolutal transfer arises from the reduction in fluid viscosity associated with higher β values. Furthermore, both heat and mass transfer decrease as the Hartmann number (Ha) increases. This behaviour is explained by the resistive Lorentz forces induced at higher Ha, which reduce the kinetic energy of the fluid particles and consequently diminish both heat and mass transfer.

4.3 Influence of Geometric Aspect Ratio, Thermal Conductivity Ratio, and Thrust Ratio Parameters

Figures 6 and 7 illustrate the impact of varying the geometric aspect ratio, thermal conductivity ratio and thrust ratio on heat and mass transfer, with the parameters set as follows: $R_{T,nf} = 10^4$, $Ha = 50$, $Pr_{nf} = 6.8$, $Le = 2.5$, $\varphi = 0.05$, $Da = 0.001$, $\xi = 5$, $R = 1$, $Sr = 1$, $Du = 1$

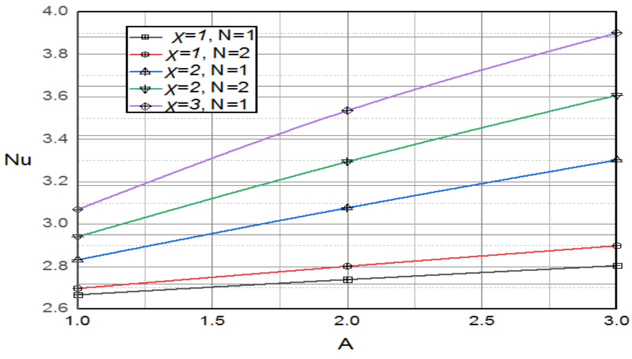

Figure 6: The effect of A, χ and N on the Nusselt Number (Nu).

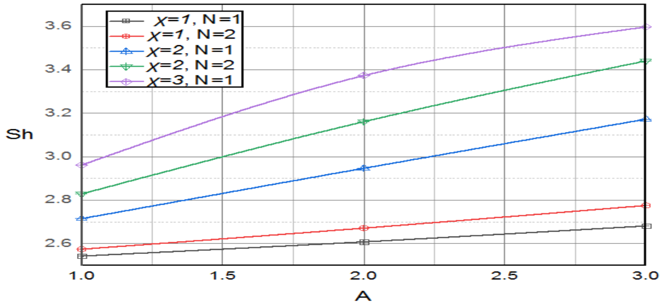

Figure 7: The effect of A, χ and N on the Sherwood Number (Sh).

The results indicate that both heat and mass transfer increase with higher values of the thermal conductivity ratio and geometric aspect ratio. This enhancement is attributed to the strengthened thermal and solutal buoyancy forces. Moreover, the figures show that as the buoyancy effects become more pronounced, the flow within the enclosure intensifies due to the combined influence of thermal and concentration-driven buoyancy, resulting in a significant increase in the average Nusselt and Sherwood numbers.

5. CONCLUSION

Natural thermosolutal convection in cylindrical cavities filled with a Casson nanofluid, under the combined influence of chemical reactions, radiation and magnetic fields, leads to the following findings:

1. Mass transfer decreases as the chemical reaction parameter increases, resulting in a reduction in species concentration.

2. Both the average Sherwood and Nusselt numbers decrease with increasing Soret and Dufour numbers, which characterise the thermodiffusion phenomenon, leading to reductions in both mass and heat transfer.

3. Heat transfer increases with the radiation parameter due to the strengthened flux intensity. In contrast, mass transfer decreases slightly with increasing radiation, which can be attributed to the enhancement of thermodiffusion effects.

4. Higher values of the Casson fluid parameter result in increased heat and mass transfer, which can be explained by the stronger flow intensity associated with higher Casson parameters.

5. Conversely, both heat and mass transfer decrease with increasing Hartmann number (Ha), with a more pronounced reduction at higher Ha values. This is caused by resistive Lorentz forces in the flow field, which reduce the kinetic energy of the fluid particles.

6. Heat and mass transfer are also enhanced by increases in the thermal conductivity ratio and geometric aspect ratio, due to the strengthening of thermal and solutal buoyancy forces.

7. Finally, the combined effects of thermal and concentration-driven buoyancy induce stronger flow within the enclosure, resulting in a notable rise in the average Nusselt and Sherwood numbers.

6. ACKNOWLEDGEMENTS

The authors would like to express their gratitude to all colleagues and institutions who contributed to this work. It should be noted that no funding or grants were received for this study.

7. REFERENCES

1. Aly, A. M., Chamkha, A. J. & Raizaha, Z. A. S. (2020). Unsteady coupled heat and mass transfer by free convection from a vertical plate embedded in porous media under impacts of radiation and chemical reaction. *J. Heat Mass Trans. Res.*, 7, 95–103.
2. Zhang, Y. & Zheng, L. (2012). Analysis of MHD thermosolutal Marangoni convection with heat generation and a first-order chemical reaction. *Chem. Eng. Sci.*, 69, 449–455. https://doi.org/10.1016/j.ces.2011.10.069
3. Al-Mudhaf, A. & Chamkha, A. J. (2005). Similarity solutions for MHD thermosolutal Marangoni convection over a flat surface in the presence of heat generation or absorption effects. *Heat Mass Trans.*, 42, 112–121. https://doi.org/10.1007/s00231-004-0611-8
4. El Hamma, M. et al. (2022). Theoretical and numerical study of thermosolutal convection in a cylindrical porous cavity filled with a nanofluid and taking into account Soret and Dufour effects. *Int. J. Eng. Appl.* (*I.R.E.A.*)., 10(1). https://doi.org/10.15866/irea.v10i1.20809
5. El Hamma, M. et al. (2022). Effect of magnetic field on thermosolutal convection in a cylindrical cavity filled with nanofluid, taking into account Soret and Dufour effects. *JPJ. Heat Mass Trans.*, 26, 1–26. https://doi.org/10.17654/0973576322009
6. Al-Sulaimi, B. (2016). The non-linear energy stability of Brinkman thermosolutal convection with reaction. *Ricerche Math.*, 65, 381–397. https://doi.org/10.1007/s11587-015-0254-8
7. Mohamed, R. A., Abo-Dahab, S. M. & Nofal, T. A. (2010). Thermal radiation and MHD effects on free convective flow of a polar fluid through a porous medium in the presence of internal heat generation and chemical reaction. *Math. Probl. Eng.*, 10, 1–27. https://doi.org/10.1155/2010/804719
8. El Hamma, M. (2024). Effects of radiation absorption, Soret and Dufour numbers on MHD thermosolutal convection in a porous cylindrical cavity filled with a Casson nanofluid. *JPJ. Heat Mass Trans.*, 37(3), 377–388. https://doi.org/10.17654/0973576324026
9. Qadan, H. et al. (2019). A theoretical study of steady MHD mixed convection heat transfer flow for a horizontal circular cylinder embedded in a micropolar Casson fluid with thermal radiation. *J. Comput. Appl. Mech.*, 50(1), 165–173. https://doi.org/10.22059/jcamech.2019.278376.372
10. Sharma, S. & Jain, S. (2024). Chemical reactions on MHD couple stress fluids towards stretchable inclined cylinder. *J. Heat Mass Trans. Res.*, 11(21), 139–150. https://doi.org/10.22075/jhmtr.2024.31241.1463
11. Patil, P. M. & Kulkarni, P. S. (2008). Effects of chemical reaction on free convective flow of a polar fluid through a porous medium in the presence of internal heat generation. *Int. J. Therm. Sci.*, 47, 1043–1054. https://doi.org/10.1016/j.ijthermalsci.2007.07.013

12. Elattari, L., Rtibi, A. & El Hamma, M. (2024). Thermosolutal convection in an inclined cylindrical cavity filled with Casson fluid in the presence of the Soret and Dufour effects. *JPJ. Heat Mass Trans.*, 37(2), 171–184. https://doi.org/10.17654/0973576324012
13. Laxmaiah, K. & Reddy, Y. D. (2025). Thermal radiation and chemical reaction effects on MHD Williamson nanofluid flow over an exponentially porous stretching sheet with non-uniform heat source/sink. *J. Radiat. Res. Appl. Sci.*, 18(3), 1–13. https://doi.org/10.1016/j.jrras.2025.101742
14. Ahad, J. I. et al. (2024). Magnetohydrodynamics thermosolutal convection of hybrid MWCNT–Fe3O4–water nanofluid along a vertical wavy surface with wall heat and mass flux. *Partial Differ. Equ. Appl. Math.*, 10, 100667. https://doi.org/10.1016/j.padiff.2024.100667
15. El Haroui, M. et al. (2017). Prediction of thermosolutal convection in a porous medium with Soret–Dufour and chemical reaction effects. *Comput. Therm. Sci.*, 9(4), 383–393. https://doi.org/10.1615/ComputThermalScien.2017019817
16. El Hamma, M. et al. (2023). Analysis of MHD thermosolutal convection in a porous cylindrical cavity filled with a Casson nanofluid, considering Soret and Dufour effects. *J. Heat Mass Trans. Res.*, 10(2), 197–206. https://doi.org/10.22075/jhmtr.2023.30532.1439
17. Choukairy, K. & Bennacer, R. (2012). Numerical and analytical analysis of the thermosolutal convection in a heterogeneous porous cavity. *Fluid Dyn. Mater. Processing*, 8(2), 155–172. https://doi.org/10.3970/fdmp.2012.008.155
18. Venkatadri, K. et al. (2020). Influence of magnetic wire positions on free convection of Fe3O4–water nanofluid in a square enclosure utilizing MAC algorithm. *J. Comput. Appl. Mecha.*, 51(2), 323–331. https://doi.org/10.22059/jcamech.2019.288693.426
19. Swapna, D. et al. (2023). Viscous dissipation and chemical reaction on radiative MHD Casson nanofluid past a stretching surface with a slip effect. *J. Heat Mass Trans. Res.*, 10(2), 315–328. https://doi.org/10.22075/jhmtr.2024.31758.1477
20. Hussein, A. K. et al. (2024). MHD mixed convection flow of alumina–water nanofluid into a lid-driven cavity with different patterns of wavy sidewalls. *J. Comput. Appl. Mecha.*, 55(1), 92–112. https://doi.org/10.22059/jcamech.2024.369622.922
21. Essalhi, H., Tadili, R. & Bargach, M. N. (2018). Comparison of thermal performance between two solar air collectors for an indirect solar dryer. *J. Phys. Sci.*, 29(3), 55–65. https://doi.org/10.21315/jps2018.29.3.5
22. Zhu, Z. & Chen, J. (2022). Numerical methods for unsteady convection–diffusion problems based on combining compact difference schemes with Runge–Kutta methods. *J. Phys. Sci.*, 33(1), 1–15. https://doi.org/10.21315/jps2022.33.1.1
23. Turabi, Y. U. B. et al. (2025). Natural convective flow of hybrid nanofluid in a triangular enclosure with heated wavy wall and cold obstacle. *Case Stud. Therm. Eng.*, 73, 106515. https://doi.org/10.1016/j.csite.2025.106515
24. Ahmad, S. et al. (2024). Numerical simulation of magnetohydrodynamics double-diffusive natural convection in a cavity with non-uniform heated walls. *Appl. Therm. Eng.*, 253, 123778. https://doi.org/10.1016/j.applthermaleng.2024.123778
25. Munir, S. & Turabi, Y. U. B. (2025). Impact of heated wavy wall and hybrid nanofluid on natural convection in a triangular enclosure with embedded cold cylinder under inclined magnetic field. *Arab. J. Sci. Eng.*, 50, 4007–4020. https://doi.org/10.1007/s13369-024-09450-3
26. Patankar, S. V. (1980). Numerical heat transfer and fluid flow. New York: Hemisphere.

27. Bounouar, A. et al. (2016). Numerical and mathematical modeling of unsteady heat transfer within a spherical cavity: Applications laser in medicine. *Contemporary Eng. Sci.*, 9(24), 1183–1199. https://doi.org/10.12988/ces.2016.67118
28. Sammouda, M. (2012). *Modélisation théorique et numérique du phénomène de la convection naturelle et thermosolutale dans les milieux poreux à porosité variable*. PhD diss., Université Mohamed V., Morocco.
29. Frankel, S. P. (1950). Convergence rate of iterative treatments of partial differential equations. *Math. Tables Other Aids Comput.*, 4, 65–75. https://doi.org/10.2307/2002770